Quantum Confinement Effects in Materials for Daytime Radiative Cooling: An *Ab-initio* Investigation

Costanza Borghesi[1], Claudia Fabiani[2,3], Anna Laura Pisello[2,3], and Giacomo Giorgi[1,3,4(✉)]

[1] Department of Civil and Environmental Engineering (DICA), Università degli Studi di Perugia, Via G. Duranti 93, 06125 Perugia, Italy
[2] Department of Engineering, Università degli Studi di Perugia, Via G. Duranti 93, 06125 Perugia, Italy
[3] CIRIAF - Interuniversity Research Centre, University of Perugia, Perugia, Italy
anna.pisello@unipg.it, giacomo.giorgi@unipg.it
[4] CNR-SCITEC, 06123 Perugia, Italy

Abstract. We have here performed a campaign of first-principles calculations comparing the effect of confinement in two ABO_3-perovskites, $SrTiO_3$ and $BaSnO_3$. The study is motivated by the quest of novel materials for daytime radiative cooling devices, a recently suggested mechanism to passively cool down the temperature of sky facing objects (mainly buildings and constructions). In particular, after assessing the computational setup for the calculation of our structures, we have similarly calculated the bandstructure of 3D, 2D, and 0D systems. We both employed standard density functional theory and meta-GGA methods to do it and discussed pros and cons of the two approaches. Finally, we discuss the possible applicability of 0D species as materials for radiative cooling as function of a large and direct bandgap.

Keywords: Daytime radiative cooling · Density functional theory · Inorganic perovskites

1 Introduction

The dependence of energy supplies from non-renewable fossil fuels is not only accompanied by dramatic effects on the environment, but is also extremely affected by geopolitical resilience factors that largely impact on the fluctuating price and availability of such resources. In addition ∼10% of global CO_2 emissions are ascribed to cooling devices, i.e. air-conditioners (ACs), which exploit electricity produced mainly from non-renewable fossil fuels [1]. It should be similarly kept in mind that the technology of most ACs is still based on the emission of waste heat in air with subsequent outdoor temperature increase [2] and in some cases exploit hydrofluorocarbons (HFCs), i.e. greenhouse gases even more harmful than CO_2 itself. In addition to that, those compounds can last in the

© The Author(s), under exclusive license to Springer Nature Switzerland AG 2022
O. Gervasi et al. (Eds.): ICCSA 2022 Workshops, LNCS 13382, pp. 305–318, 2022.
https://doi.org/10.1007/978-3-031-10592-0_23

atmosphere up to many thousands of years and, once released into the air, they can partially dissolve into the oceans over few decades. This means that once in the atmosphere, greenhouse-gases will continue to affect climate for thousands of years. Thus, the reliance on fossil fuels and on traditional cooling devices is a twofold issue, i.e. it raises global warming while continuing to pollute the air. As a matter of fact, cooling seems to be one of the most detrimental factors in the climate crisis and things are unlikely to improve as the global population is constantly rising. This becomes even more serious in urban contexts, where currently 68% of the global population lives and are characterized by local overheating typically referred to Urban Heat Island (UHI) [3]. Such phenomenon is probably the best documented one as related to climate change with a clear anthropogenic responsibility imputable to vehicular traffic emissions, urban solar trapping, low solar reflectivity and evapotraspiration potential of built environment [4]. UHI may indeed reach out up to 10K air temperature increase and important relative humidity decrease [4], as registered in whole urban contexts and in microclimate granularity [5]. The community should thus proceed in two parallel directions both paying attention on optimizing efficient and renewables exploitation [6–22] as in the last few decades, but also finding strategies to manage urban overheating by means of adaptation and mitigation actions. A mitigative approach to reduce cooling energy consumption and UHI has been recently proposed and is based on the exploitation of a well-known phenomenon that is the radiative cooling [23–30]. At nighttime radiative cooling occurs naturally and takes advantage on the fact that any outdoor, sky facing, object may emit a significant fraction of thermal radiation into outer space through the so-called "atmospheric window" in the mid IR wavelength range (8–13 μm) [31]. The big challenge is to shift this nocturnal natural process to daytime when radiative conditions are clearly different. Unlike traditional AC systems, passive radiative cooling devices are energy-free and refrigerant-free cooling technologies that reflect incoming solar irradiance, while emitting thermal radiation to cool down the universe thereby achieving sub-ambient cooling. This self-cooling technique has demonstrated a tremendous potential, attracting significant interest from paint, air conditioning and building industries. Radiative passive cooling devices generally consist of two parts: a solar reflection layer and a radiative cooling layer [26,29]. While the reflective layer is mainly constituted by a metallic element, i.e. Ag and/or Al, the real core of the device is here represented by the radiative layer (responsible of both absorption in the VIS and emission in mid IR) which has been in the last decades a topic of deep investigation [25,32,33]. Recent technological developments enable the usage of metamaterials [33], of nanoparticle-doped systems [32], and of photonic structures [25] to maximise the efficiency of such component. Also halide perovskites, materials with remarkable optoelectronic features mainly investigated for photovoltaics [6], have been shown to play a relevant role in such architectures [34,35]. The first experimental sub-ambient daytime radiative cooling has been achieved based on this latter architecture by stacking layers of HfO_2 and SiO_2 with different thicknesses [25] and based on such architecture later flavours (TiO_2/SiO_2) were similarly suggested [36]. More

recently, based on their optical response, photoluminescent (third generation of construction materials) [37] and/or thermochromic (next generation of construction materials) [37] materials have been predicted as optimal radiative cooling materials to replace standard materials (heat-absorbers) used in constructions. Due to their intrinsic complexity, photonic/metamaterials structures are theoretically investigated by means of Maxwell Equations [38–41] and, except for a few works that recently have appeared in literature where the metrics to define a good material as an active layer for daytime passive cooling are discussed [42], the topic remains quite overlooked from the computational modelling and atomistic points of view, despite the increasing availability of more powerful computational resources and, accordingly, the reliability/accuracy of the related simulations. In this context, our aim here is to investigate at the atomistic level the active components for the radiative part and possibly predict/suggest novel materials with improved performances. In details, high entropy alloys (HEAs) [43–45] and in particular oxides (HEOs) [46] have been recently introduced as a sort of philosopher's stone in materials science. Such compounds already play a relevant role in several technological fields ranging from catalysis [47], to photocatalysis [48], ion-batteries [49], magnetism [50], and energy storage [51], to mention just a few of them. The idea that subtends their importance is the possibility of an (almost) infinite number of combinations to form compounds which are highly stabilized because of the enhanced role played by the entropic factor (ΔS_{mix}) in the Gibbs free energy equation. Our focus is a material which embodies the optimal features that characterise the radiative cooling material in terms of absorption/emission. Accordingly, with the idea of applying HEOs to radiative cooling processes, our initial investigation is here devoted to the individuation and the analysis of candidate materials aiming to establish relationships between their structural and electronic features. Keeping in mind that the dimensionality of the radiative cooling materials is crucial for the final working principle of the device, we here provide an initial analysis about $BaSnO_3$ (hereafter also BSO) –whose applicability in the field seems quite promising and whose flexible perovskite structure can be used as network for a HEO– and its low dimensional counterparts, and compare their properties with those of another well assessed and more investigated perovskite oxide, i.e. $SrTiO_3$ (hereafter also STO).

2 Computational Details

By means of Density Functional Theory methods as implemented in the VASP code [52–55], we performed a campaign of calculations on the two previously mentioned systems, $SrTiO_3$ and $BaSnO_3$. In such simulations the electron exchange-correlation functional of Perdew, Burke, and Ernzerhof (PBE) [56] was used. The projector augmented wave (PAW) method [57,58] has been similarly adopted using a cutoff energy of 500 eV for the plane-wave basis set. For the geometry optimization the Brillouin Zone (BZ) was sampled by means of a Γ-centred $6 \times 6 \times 6$ mesh (more dense meshes are used for electronic properties calculations). Optimization of lattice parameters and ionic positions ended

when residual forces were lower than 5×10^{-4} eV/Å. Due to the shortcomings associated with the DFT in predicting excited state properties, we first calculated the bandstructure at the DFT level and then to improve the agreement with the experiments we tested several other post-DFT methods with particular attention to the modified Becke-Johnson (mBJ) meta-GGA functional [59,60]. Such potential-only functional provides in principle results of electronic properties in good agreement with those typical of a *GW* run but at a very lower computational cost.

3 Results and Discussion

Both STO and BSO belong to the ABO_3-type perovskite crystals. Following the Goldschmidt tolerance factor, t, the empirical factor widely used over the years as a criterion for discussing the stability of perovskites [61],

$$t = \frac{R_A + R_B}{\sqrt{2}(R_B + R_O)} \tag{1}$$

where R_A, R_A, and R_A are the ionic radius for the A-site, B-site, and oxide ions [62], respectively, two values very close to the unity are predicted (1.01 and 1.02, for $SrTiO_3$ and $BaSnO_3$) assessing the ideally cubic geometry of the two systems. $SrTiO_3$ is cubic (Pm3m, space group 221) at room temperature and for ordinary pressure, undergoing phase transitions towards tetragonal ($I_{4/mcm}$, s.g. 140) and orthorhombic (Cmcm, s.g. 63) polymorphs at increasing pressure values [63]. Our optimized structure (see Fig. 1) is characterized by a lattice parameter ($a = 3.95\,\mathring{A}$) which is consistent with other values reported in literature (see Table 1) We then optimized the structure of BSO. Similarly to STO, bulk BSO experimentally crystallizes in the cubic perovskite structure Pm3m. The calculated lattice parameter is 4.186 Å in pretty good agreement with previously reported data (see Fig. 1). To stress that in BSO Ba atom (A-site cation) occupies the center of the cell (0.5; 0.5; 0.5), while in STO the same A-site ion, here Sr, occupies the corner (0.0; 0.0; 0.0) [64]. For the sake of comparison, in Fig. 1 we put the A-site at the corner and the B-site cation in the center of the cell, respectively.

On such optimized systems we calculated the bandstructures that are depicted in Fig. 2. As for the structural ones, the main electronic properties for both bulk STO and BSO are similarly reported in Table 1 As widely reported the bandgap of these two bulk materials is indirect ($R \rightarrow \Gamma$) and in this sense their applicability in radiative cooling devices could be potentially less efficient since they are expected to re-emit (compared to a direct-gap material) more slowly with possible heating of the material. In details, the gap calculated at the DFT level is 1.387 eV for STO and 0.218 eV for BSO. As well-known the DFT calculated value massively underestimates the experimental one. It is worth stressing that we used a reduced number of electrons in the valence of the B-site cation pseudopotentials. For both Sn and Ti indeed we used 4 electrons that we realized

Table 1. Optimized lattice parameter a and electronic bandgap at different levels of theory obtained in the present work. For the sake of comparison same data, experimental and theoretical, from previous literature are reported.

	$SrTiO_3$	$BaSnO_3$
a (Å)	3.95 (present work)	4.186 (present work)
	3.92 [63] (theo. PW91)	4.055 [65] (theo. GGA)
	3.95 [66] (theo GGA PW)	4.156 (Sn: no semicore) [67] (theo PBE)
	3.94 [66] (theo PBE PW)	4.186 (Sn semicore) [67] (theo PBE)
	3.90 [68] (exp.)	4.19903 [69] (theo FP-LAPW)
		4.115 [70] (exp.); 4.1194 [69] (exp)
E_{gap} (eV)	1.387 (R $\rightarrow$ Γ, this work, PAW/PBE)	0.218 (R $\rightarrow$ Γ, this work, PAW/PBE)
	1.722 ($\Gamma \rightarrow \Gamma$, this work, PAW/PBE)	0.761($\Gamma \rightarrow \Gamma$, this work, PAW/PBE)
	2.355 (R $\rightarrow$ Γ, this work, PAW/mBJ)	3.593 (R $\rightarrow$ Γ, this work, PAW/mBJ)
	2.626 (R $\rightarrow$ Γ, this work, PAW/mBJ)	3.885 (R $\rightarrow$ Γ, this work, PAW/mBJ)
	3.25 [71] (exp)	0.4 [69] (R $\rightarrow$ Γ, (theo FP-LAPW)
		3.56 [72] (exp); 3.4 [73](exp)

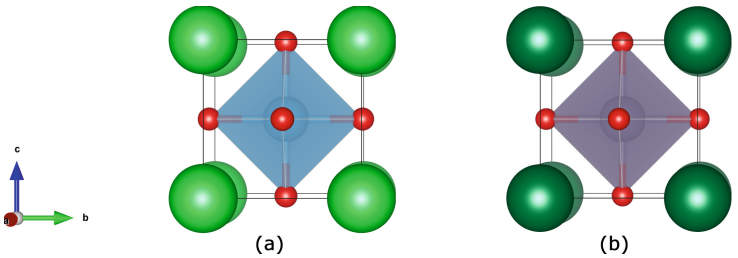

Fig. 1. Optimized structures for (a) STO and (b) BSO. [Light green, Sr; cyan: Ti; red: O; dark green: Ba; grayish: Sn atoms.] (Color figure online)

to slightly underestimate our DFT gap if compared with other previously calculated gaps at the same level of theory (using 10 electrons in the valence for Ti atoms in STO opens the gap of ∼0.3 eV) On the other hand, once we apply the mBJ potential to correct the gap we observe a two-fold behavior. Indeed, mBJ opens STO gap but not sufficiently to recover the experimental value (2.355 eV), while in the case of BSO mBJ tends to recover (3.593 eV) the experimentally reported values (∼3.5 eV) [72,73]. By means of a basic computational setup we similarly calculated the *one-shot* G_0W_0 bandgap for the two bulk systems. For STO, in particular, the *one-shot* G_0W_0 leads to a (still R $\rightarrow$ Γ) gap of 3.08 eV, not that far from the experimentally reported value of 3.25 eV [71]. In the case of BSO, the same G_0W_0 bandgap is 2.95 eV revealing at opposite the need of other iterations to reach the agreement with the experimental bandgap value [72,73].

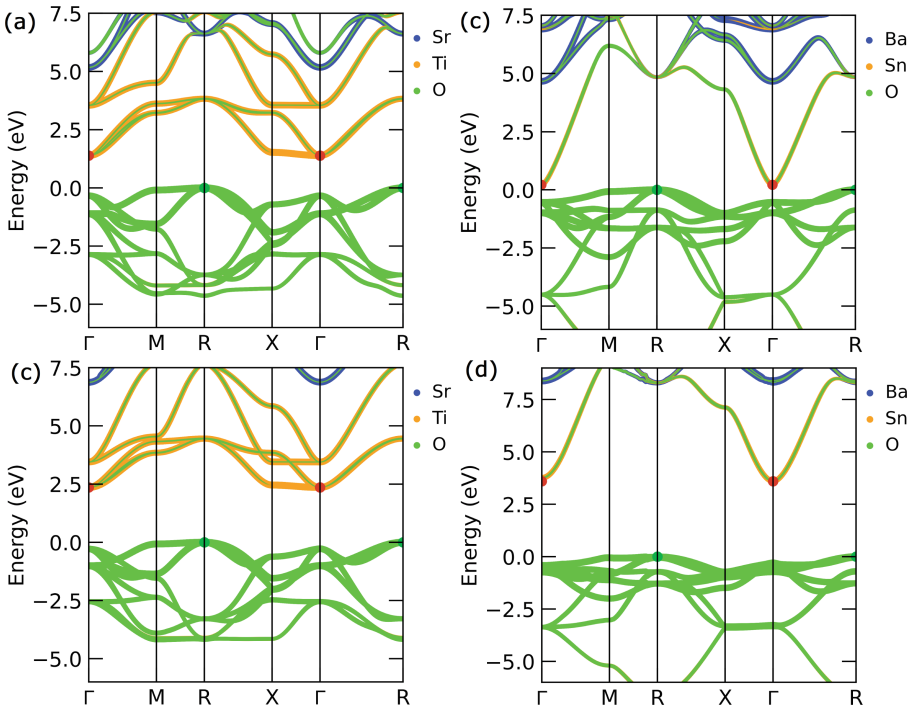

Fig. 2. DFT calculated bandstructure for (a) STO and (b) BSO. Same, but calculated at the mBJ level of theory in (c) and (d)

In view of the possible applications of $BaSO_3$ compound family in radiative cooling devices, we then focus on the structural confinement of the investigated systems by reducing their dimensionality. The most immediate and natural way to do it is the analysis of the so-called Ruddlesden-Popper (RP) phases. Recently, such mixed 2D/3D and pure 2D systems have gained particular attention because of their hybrid organic-inorganic halide counterparts which have been shown to play a main role in photoconversion processes [74–78]. In the case of STO, such RP phases – with stoichiometric relationship $Sr_{n+1}Ti_nO_{3n+1}$ – are characterized by the insertion of additional SrO planes into the perovskite lattice to form quantum wells of variable thicknesses. STO RP phases have tetragonal structure with $I_{4/mmm}$ symmetry (s.g. 139, $Z = 2$), We studied the initial members of the series $n = 1 - 3$ for both STO and BSO, i.e. the pure 2D system ($n = 1$) and the first two members of the mixed 2D/3D class. While the former compounds (STO RP phases) are well assessed and already investigated [79] with particular focus on structural, electronic and optical features [80,81], the latter (BSO) are only hypothetical compounds that we obtained based on the STO RP structural counterparts [82]. We want to here stress that the modellization of such $n = 1-3$ STO (and consequently BSO) RPs stems from the structures reported in the Materials Project website [64] and that no fine tuning of atomic positions have

been performed. The resulting optimized geometries of the hypothetical BSO RP phases ($n = 1 - 3$) are reported in Fig. 3.

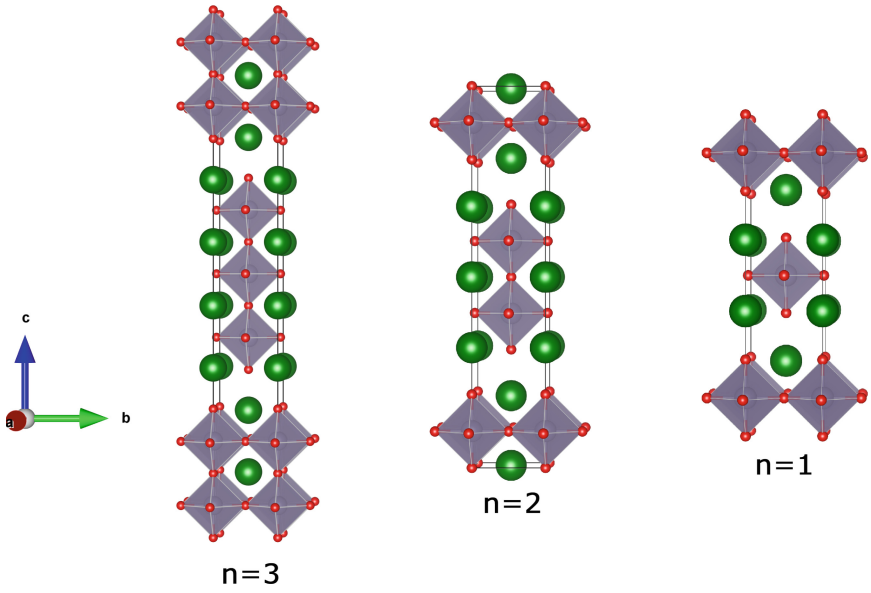

Fig. 3. DFT optimized structures for BSO RP phase ($n = 1 - 3$) [Dark green, Ba; grayish: Sn; red: O atoms]. (Color figure online)

Concerning the electronic features of such dimensionally reduced systems, in Fig. 4 we show the trend of quantum confinement effects in both STO RP and BSO RP phases and at the PBE and mBJ level of theory, respectively. As expected the reduction of the layer thickness ($n = 3 \rightarrow n = 1$) is associated with an increase of the bandgap. On the other hand, compared with PBE, the confinement effect are less marked for increasing values of n in both cases, an effect which is more noticeable in the case of BSO RP phases. Indeed, passing from $n = 2$ to $n = 1$ in BSO RP (STO RP) is associated with an increase in the gap of 34% (9%) at the PBE level of theory, from 1.640 eV to 2.488 eV (from 1.488 to 1.636 eV). The same relative bandgap increase at the mBJ level for BSO RP is halved to 15% (4.392 eV to 5.189 eV), while for STO RP the same variation is only of 6.5% (from 2.082 to 2.227 eV). All the calculations here refer to an indirect bandgap, which is the minimal one for all the investigated STO and BSO RP phases.

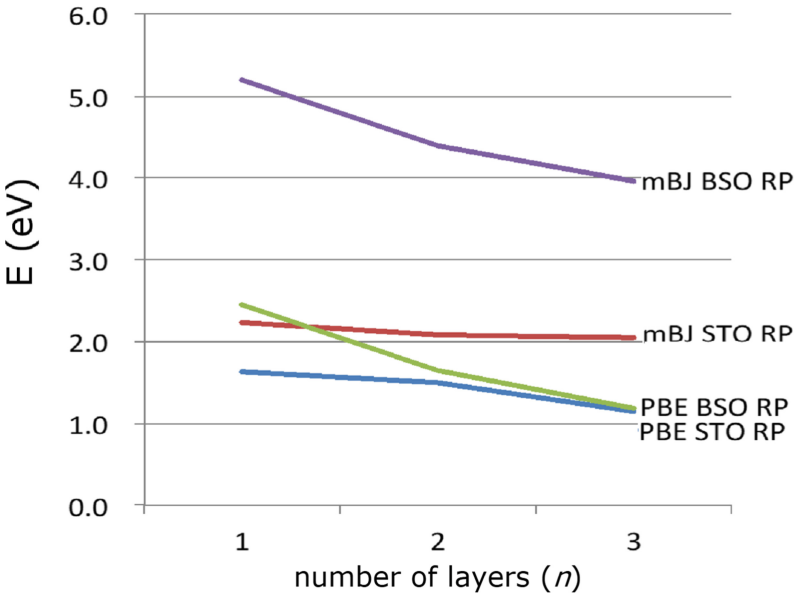

Fig. 4. Indirect (smallest) bandgap variation for the first three terms $n = 1 - 3$ of the $Sr_{n+1}Ti_nO_{3n+1}$ and $Ba_{n+1}Sn_nO_{3n+1}$ Ruddlesden-Popper phases.

The last dimensionality we want to discuss here is the 0D counterpart of both STO and BSO. Such systems are structurally characterized by the presence of isolated MO_6 octahedra (M = Ti, Sn). Now, considering the lack of literature about such systems (other 0D oxide perovskites have been investigated) [83,84] we moved from a well-assessed and investigated 0D halide perovskite (Cs_4PbBr_6) [64], replacing anion and cation positions with those of interest here, and finally fully optimized lattice parameters and ionic positions. Thus, in the 0D case both systems are theoretically engineered. As expected the value of the gap is in this case the largest one (2.809 and 2.471 eV at the PBE level, and 3.751 and 6.240 eV at the mBJ level for 0D STO and 0D BSO, respectively). The optimized structures for such systems along with bandstructures –the latter ones calculated at both level of theory– are reported in Fig. 5. Remarkably, mBJ once more shows a less marked tendency in opening the bandgap compared to the PBE level (2.809 → 3.751 eV) for the case of 0D STO, while the correction is massive (2.471 → 6.240 eV) for 0D BSO. It is worth stressing that Tong et al. [42] have predicted an enhanced efficiency as material for radiative cooling for all those that have an electronic bandgap larger than 4.13 eV, i.e. energy upper bound in solar spectrum, but smaller than that of $BaSO_4$ (another material of interest in radiative cooling oriented applications) which is 7.27 eV [42]. In this context, our 0D BSO would perfectly fit the electronic requirement, with the even more appealing feature to be a *direct* gap ($\Gamma \rightarrow \Gamma$) material which in principle should make the material able to more easily emit in the sky-window region. The other

metrics the material should satisfy to be relevant for such applications is the phonon bandstructure with particular focus in the 8–13 μm region. Calculations in this sense are nowadays in progress.

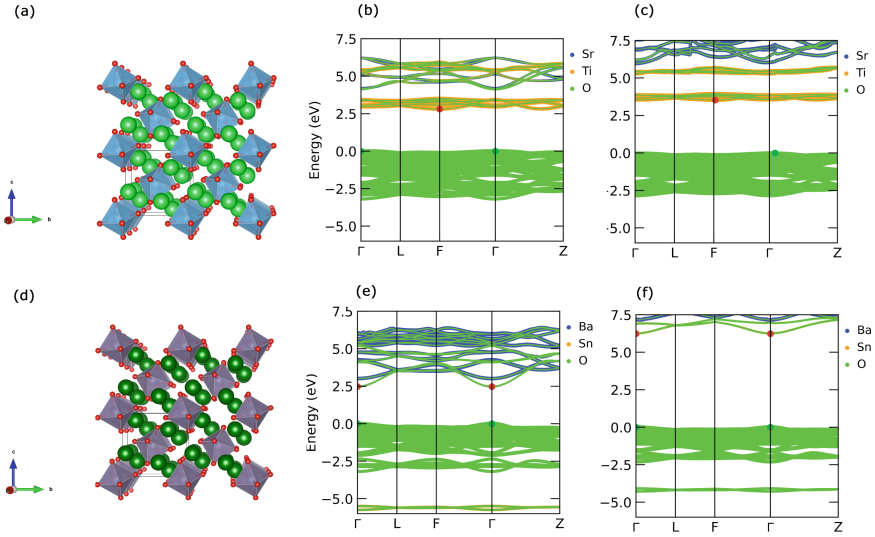

Fig. 5. 2×2 supercell of the optimized structure of (a) 0D $SrTiO_3$, (b) PBE calculated, and (c) mBJ calculated bandstructure. Same (d–f) for 0D $BaSnO_3$

4 Remarks

Aiming at investigating materials with applicability in radiative cooling devices, we here did an exploratory initial campaign of calculations from first-principles on the size reduction of two ABO_3-type perovskites comparing the features of the well-assessed and investigated $SrTiO_3$ and those of the tin-based $BaSnO_3$ compound. We paid attention on both bulk and on the first three terms ($n = 1 - 3$) of their related Ruddlesden-Popper phases, i.e. $A_{n+1}B_nO_{3n+1}$. Despite a very good agreement between our obtained structural parameters and previous experimental and theoretical reported ones for bulk, we note that treating the B-site cation (both Ti and Sn) with a reduced electron numbers in the valence induces a physiological contraction of their calculated bandgap, suggesting that for a very accurate prediction of the electronic and optical features the number of electrons in the valence for B-site ions must be larger than four. On the other hand we obtain a quite interesting trend: the confinement effects seem to be more noticeable in the case of $BaSnO_3$ while still interesting is the fact that the theoretically predicted zero-dimensional $BaSnO_3$ systems, i.e. Ba_4SnO_6 is the only direct (and large) bandgap material which is preferable because of a facile absorption/emission associated with possible heat reduction (purely radiative

mechanism). The present is a preliminary investigation that mandatory needs further analysis, testing different pseudopotentials and calculating phonon features, and we are already working in such directions with the final aim of developing a new disruptive mitigation technique to face the urban heat island issue.

Acknowledgments. The authors thank the ERC Stg Project HELIOS (GA 101041255, PI dr. A.L. Pisello) funded by the European Union. Views and opinions expressed are however those of the author(s) only and do not necessarily reflect those of the European Union or the European Research Council. Neither the European Union nor the granting authority can be held responsible for them. G.G. and C.B. acknowledge ISCRA B, and C initiatives for awarding access to computing resources on m100 at CINECA SuperComputer Center, Italy. G.G. thanks the Dipartimento di Ingegneria Civile e Ambientale of the University of Perugia for allocated computing time within the project "Dipartimenti di Eccellenza 2018–2022". Authors are similarly grateful to Prof. L. Latterini (Dept of Chemistry, Biology and Biotechnology, Perugia University) for the very fruitful scientific discussions.

References

1. Mutschler, R., Rüdisüli, M., Heer, P., Eggimann, S.: Benchmarking cooling and heating energy demands considering climate change, population growth and cooling device uptake. Appl. Ener. **288**, 116636 (2021)
2. Calm, J.M.: Emissions and environmental impacts from air-conditioning and refrigeration systems. Int. J. Refrig. **25**(3), 293–305 (2002)
3. Fabiani, C., Pisello, A.L., Bou-Zeid, E., Yang, J., Cotana, F.: Adaptive measures for mitigating urban heat islands: the potential of thermochromic materials to control roofing energy balance. Appl. Ener. **247**, 155–170 (2019)
4. Paolini, R., et al.: The hygrothermal performance of residential buildings at urban and rural sites: Sensible and latent energy loads and indoor environmental conditions. Energ. Build. **152**, 792–803 (2017)
5. Kousis, I., Pigliautile, I., Pisello, A.L.: Intra-urban microclimate investigation in urban heat island through a novel mobile monitoring system. Sci. Rep. **11**(1), 1–17 (2021)
6. Kojima, A., Teshima, K., Shirai, Y., Miyasaka, T.: Organometal halide perovskites as visible-light sensitizers for photovoltaic cell. J. Am. Chem. Soc. **131**(17), 6050–6051 (2009)
7. Giorgi, G., Fujisawa, J.-I., Segawa, H., Yamashita, K.: Small photocarrier effective masses featuring ambipolar transport in methylammonium lead iodide perovskite: a density functional analysis. J. Phys. Chem. Lett. **4**(24), 4213–4216 (2013)
8. Giorgi, G., Fujisawa, J.-I., Segawa, H., Yamashita, K.: Cation role in structural and electronic properties of 3D organic-inorganic halide perovskites: a DFT analysis. J. Phys. Chem. C **118**(23), 12176–12183 (2014)
9. Kawai, H., Giorgi, G., Marini, A., Yamashita, K.: The mechanism of slow hot-hole cooling in lead-iodide perovskite: first-principles calculation on carrier lifetime from electron-phonon interaction. Nano Lett. **15**(5), 3103–3108 (2015)
10. Giorgi, G., Yamashita, K.: Organic-inorganic halide perovskites: an ambipolar class of materials with enhanced photovoltaic performances. J. Mater. Chem. A **3**(17), 8981–8991 (2015)

11. Giorgi, G., Fujisawa, J.-I., Segawa, H., Yamashita, K.: Organic-inorganic hybrid lead iodide perovskite featuring zero dipole moment guanidinium cations: a theoretical analysis. J. Phys. Chem. C **119**(9), 4694–4701 (2015)
12. Hata, T., Giorgi, G., Yamashita, K.: The effects of the organic-inorganic interactions on the thermal transport properties of $CH_3NH_3PbI_3$. Nano Lett. **16**(4), 2749–2753 (2016)
13. Giorgi, G., Yamashita, K.: Alternative, lead-free, hybrid organic-inorganic perovskites for solar applications: a DFT analysis. Chem. Lett. **44**(6), 826–828 (2015)
14. Giorgi, G., Yamashita, K.: Zero-dimensional hybrid organic-inorganic halide perovskite modeling: insights from first principles. J. Phys. Chem. Lett. **7**(5), 888–899 (2016)
15. Giorgi, G., Yamashita, K.: Zero-dipole molecular organic cations in mixed organic-inorganic halide perovskites: possible chemical solution for the reported anomalous hysteresis in the current-voltage curve measurements. Nanotechnology **26**(44), 442001 (2015)
16. Hata, T., Giorgi, G., Yamashita, K., Caddeo, C., Mattoni, A.: Development of a classical interatomic potential for $MAPbBr_3$. J. Phys. Chem. C **121**(7), 3724–3733 (2017)
17. Palummo, M., Varsano, D., Berríos, E., Yamashita, K., Giorgi, G.: Halide PB-free double-perovskites: ternary vs. quaternary stoichiometry. Energies **13**(14), 3516 (2020)
18. Giorgi, G., Yoshihara, T., Yamashita, K.: Structural and electronic features of small hybrid organic-inorganic halide perovskite clusters: a theoretical analysis. Phys. Chem. Chem. Phys. **18**(39), 27124–27132 (2016)
19. Manzhos, S., Giorgi, G., Lüder, J., Ihara, M.: Modeling of plasmonic properties of nanostructures for next generation solar cells and beyond. Adv. Phys. X **6**(1), 1908848 (2021)
20. Giorgi, G.: Structural and electronic features of $Si/CH_3NH_3PbI_3$ interfaces with optoelectronic applicability: Insights from first-principles. Nano Energy **67**, 104166 (2020)
21. Giorgi, G., Yamashita, K., Segawa, H.: First-principles investigation of the Lewis acid-base adduct formation at the methylammonium lead iodide surfaces. Phys. Chem. Chem. Phys. **20**(16), 11183–11195 (2018)
22. Manzhos, S., et al.: Materials design and optimization for next-generation solar cell and light-emitting technologies. J. Phys. Chem. Lett. **12**(19), 4638–4657 (2021)
23. Catalanotti, S., Cuomo, V., Piro, G., Ruggi, D., Silvestrini, V., Troise, G.: The radiative cooling of selective surfaces. Sol. Energy **17**(2), 83–89 (1975)
24. Granqvist, C.G., Hjortsberg, A.: Radiative cooling to low temperatures: general considerations and application to selectively emitting SiO films. J. Appl. Phys. **52**(6), 4205–4220 (1981)
25. Raman, A.P., Anoma, M.A., Zhu, L., Rephaeli, E., Fan, S.: Passive radiative cooling below ambient air temperature under direct sunlight. Nature **515**(7528), 540–544 (2014)
26. Rephaeli, E., Raman, A., Fan, S.: Ultrabroadband photonic structures to achieve high-performance daytime radiative cooling. Nano Lett. **13**(4), 1457–1461 (2013)
27. Hossain, Md.M., Gu, M.: Radiative cooling: principles, progress, and potentials. Adv. Sci. **3**(7), 1500360 (2016)
28. Kou, J.-L., Jurado, Z., Chen, Z., Fan, S., Minnich, A.J.: Daytime radiative cooling using near-black infrared emitters. ACS Photon. **4**(3), 626–630 (2017)
29. Zhao, B., Hu, M., Ao, X., Chen, N., Pei, G.: Radiative cooling: a review of fundamentals, materials, applications, and prospects. Appl. Energy **236**, 489–513 (2019)

30. Li, Z., Chen, Q., Song, Y., Zhu, B., Zhu, J.: Fundamentals, materials, and applications for daytime radiative cooling. Adv. Mater. Technol. **5**(5), 1901007 (2020)
31. Li, W., Dong, M., Fan, L., John, J.J., Chen, Z., Fan, S.: Nighttime radiative cooling for water harvesting from solar panels. ACS Photon. **8**(1), 269–275 (2020)
32. Huang, Z., Ruan, X.: Nanoparticle embedded double-layer coating for daytime radiative cooling. Int. J. Heat Mass Transfer **104**, 890–896 (2017)
33. Zhai, Y., et al.: Scalable-manufactured randomized glass-polymer hybrid metamaterial for daytime radiative cooling. Science **355**(6329), 1062–1066 (2017)
34. Jeon, S., et al.: Multifunctional daytime radiative cooling devices with simultaneous light-emitting and radiative cooling functional layers. ACS Appl. Mater. Interfaces **12**(49), 54763–54772 (2020)
35. Son, S., et al.: Colored emitters with silica-embedded perovskite nanocrystals for efficient daytime radiative cooling. Nano Energy **79**, 105461 (2021)
36. Kecebas, M.A., Menguc, M.P., Kosar, A., Sendur, K.: Passive radiative cooling design with broadband optical thin-film filters. J. Quant. Spectrosc. Radiat. Transf. **198**, 179–186 (2017)
37. Garshasbi, S., Santamouris, M.: Using advanced thermochromic technologies in the built environment: recent development and potential to decrease the energy consumption and fight urban overheating. Sol. Energy Mater. Sol. Cells **191**, 21–32 (2019)
38. Taflove, A., Hagness, S.C., Piket-May, M.: Computational electromagnetics: the finite-difference time-domain method. Electr. Eng. Handb. **3**, 629–670 (2005)
39. Taflove, A., Brodwin, M.E.: Numerical solution of steady-state electromagnetic scattering problems using the time-dependent Maxwell's equations. IEEE Trans. Microw. Theory Tech. **23**(8), 623–630 (1975)
40. Yee, K.: Numerical solution of initial boundary value problems involving Maxwell's equations in isotropic media. IEEE Trans. Antennas Propag. **14**(3), 302–307 (1966)
41. Vinattieri, A., Giorgi, G.: Halide perovskites for photonics: recent history and perspectives. In: Halide Perovskites for Photonics, vol. 1, pp. 1–28. AIP Publishing LLC, Melville (2021)
42. Tong, Z., Peoples, J., Li, X., Yang, X., Bao, H., Ruan, X.: Atomistic characteristics of ultra-efficient radiative cooling paint pigments: the case study of $BaSO_4$. Mater. Today Phys. **24**, 100658 (2022)
43. Tsai, M.-H., Yeh, J.-W.: High-entropy alloys: a critical review. Mater. Res. Lett. **2**(3), 107–123 (2014)
44. George, E.P., Raabe, D., Ritchie, R.O.: High-entropy alloys. Nat. Rev. Mater. **4**(8), 515–534 (2019)
45. Ye, Y.F., Wang, Q., Lu, J., Liu, C.T., Yang, Y.: High-entropy alloy: challenges and prospects. Mater. Today **19**(6), 349–362 (2016)
46. Rost, C.M., et al.: Entropy-stabilized oxides. Nat. Commun. **6**(1), 1–8 (2015)
47. Albedwawi, S.H., AlJaberi, A., Haidemenopoulos, G.N., Polychronopoulou, K.: High entropy oxides-exploring a paradigm of promising catalysts: a review. Mater. Des. **202**, 109534 (2021)
48. Edalati, P., Wang, Q., Razavi-Khosroshahi, H., Fuji, M., Ishihara, T., Edalati, K.: Photocatalytic hydrogen evolution on a high-entropy oxide. J. Mater. Chem. A **8**(4), 3814–3821 (2020)
49. Zhao, C., Ding, F., Lu, Y., Chen, L., Hu, Y.-S.: High-entropy layered oxide cathodes for sodium-ion batteries. Angew. Chem. Int. Ed. **59**(1), 264–269 (2020)
50. Witte, R., et al.: High-entropy oxides: an emerging prospect for magnetic rare-earth transition metal perovskites. Phys. Rev. Mater. **3**(3), 034406 (2019)

51. Sarkar, A., et al.: High entropy oxides for reversible energy storage. Nat. Commun. **9**(1), 1–9 (2018)
52. Kresse, G., Hafner, J.: Ab initio molecular dynamics for open-shell transition metals. Phys. Rev. B **48**(17), 13115–13118 (1993)
53. Kresse, G., Hafner, J.: Ab initio molecular-dynamics simulation of the liquid-metal-amorphous-semiconductor transition in germanium. Phys. Rev. B **49**(20), 14251–1426 (1994)
54. Kresse, G., Furthmüller, J.: Efficiency of ab-initio total energy calculations for metals and semiconductors using a plane-wave basis set. Comput. Mater. Sci. **6**(1), 15–50 (1996)
55. Kresse, G., Furthmüller, J.: Efficient iterative schemes for ab initio total-energy calculations using a plane-wave basis set. Phys. Rev. B **54**(16), 11169–11186 (1996)
56. Perdew, J.P., Burke, K., Ernzerhof, M.: Generalized gradient approximation made simple. Phys. Rev. Lett. **77**(18), 3865–3868 (1996)
57. Blöchl, P.E.: Projector augmented-wave method. Phys. Rev. B **50**, 17953 (1994)
58. Kresse, G., Joubert, D.: From ultrasoft pseudopotentials to the projector augmented-wave method. Phys. Rev. B **59**, 1758 (1999)
59. Becke, A.D., Johnson, E.R.: A simple effective potential for exchange. J. Chem. Phys. **124**(22), 221101 (2006)
60. Tran, F., Blaha, P.: Accurate band gaps of semiconductors and insulators with a semilocal exchange-correlation potential. Phys. Rev. Lett. **102**(22), 226401 (2009)
61. Goldschmidt, V.M.: Die gesetze der krystallochemie. Naturwissenschaften **14**(21), 477–485 (1926)
62. Shannon, R.D.: Revised effective ionic radii and systematic studies of interatomic distances in halides and chalcogenides. Acta Crystallogr. A **32**(5), 751–767 (1976)
63. Hachemi, A., Hachemi, H., Ferhat-Hamida, A., Louail, L.: Elasticity of $SrTiO_3$ perovskite under high pressure in cubic, tetragonal and orthorhombic phases. Phys. Scr. **82**(2), 025602 (2010)
64. Jain, A., et al.: Commentary: the materials project: a materials genome approach to accelerating materials innovation. APL Mater. **1**(1), 011002 (2013)
65. Moreira, E., et al.: Structural and optoelectronic properties, and infrared spectrum of cubic $BaSnO_3$ from first principles calculations. J. Appl. Phys. **112**(4), 043703 (2012)
66. Piskunov, S., Heifets, E., Eglitis, R.I., Borstel, G.: Bulk properties and electronic structure of $SrTiO_3$, $BaTiO_3$, $PbTiO_3$ perovskites: an ab initio HF/DFT study. Comput. Mater. Sci. **29**(2), 165–178 (2004)
67. Bévillon, É., Chesnaud, A., Wang, Y., Dezanneau, G., Geneste, G.: Theoretical and experimental study of the structural, dynamical and dielectric properties of perovskite $BaSnO_3$. J. Phys.: Condens. Matter **20**(14), 145217 (2008)
68. Abramov, Y.A., Tsirelson, V.G., Zavodnik, V.E., Ivanov, S.A., Brown, I.D.: The chemical bond and atomic displacements in $SrTiO_3$ from X-ray diffraction analysis. Acta Crystallogr. B **51**(6), 942–951 (1995)
69. Farfán, J.C., Rodriguez, J.A., Fajardo, F., Lopez, E.V., Tellez, D.A.L., Roa-Rojas, J.: Structural properties, electric response and electronic feature of $BaSnO_3$ perovskite. Physica B **404**(18), 2720–2722 (2009)
70. Mountstevens, E.H., Attfield, J.P., Redfern, S.A.T.: Cation-size control of structural phase transitions in tin perovskites. J. Phys.: Condens. Matter **15**(49), 8315 (2003)
71. Van Benthem, K., Elsässer, C., French, R.H.: Bulk electronic structure of $SrTiO_3$: experiment and theory. J. Appl. Phys. **90**(12), 6156–6164 (2001)

72. Shan, C., et al.: Optical and electrical properties of sol-gel derived $Ba_{1-x}La_xSnO_3$ transparent conducting films for potential optoelectronic applications. J. Phys. Chem. C **118**(13), 6994–7001 (2014)
73. Lebens-Higgins, Z., et al.: Direct observation of electrostatically driven band gap renormalization in a degenerate perovskite transparent conducting oxide. Phys. Rev. Lett. **116**(2), 027602 (2016)
74. Smith, I.C., Hoke, E.T., Solis-Ibarra, D., McGehee, M.D., Karunadasa, H.I.: A layered hybrid perovskite solar-cell absorber with enhanced moisture stability. Angew. Chem. Int. Ed. **53**(42), 11232–11235 (2014)
75. Tsai, H., et al.: High-efficiency two-dimensional Ruddlesden-Popper perovskite solar cells. Nature **536**(7616), 312–316 (2016)
76. Palummo, M., Postorino, S., Borghesi, C., Giorgi, G.: Strong out-of-plane excitons in 2D hybrid halide double perovskites. Appl. Phys. Lett. **119**(5), 051103 (2021)
77. Giorgi, G., Yamashita, K., Palummo, M.: Nature of the electronic and optical excitations of Ruddlesden-Popper hybrid organic-inorganic perovskites: the role of the many-body interactions. J. Phys. Chem. Lett. **9**(19), 5891–5896 (2018)
78. Folpini, G., et al.: Band splitting and plurality of excitons in Ruddlesden-Popper metal halides. ChemRxiv 10.26434/chemrxiv-2021-qcm36-v2 (2021)
79. Ruddlesden, S.N., Popper, P.: The compound $Sr_3Ti_2O_7$ and its structure. Acta Crystallogr. **11**(1), 54–55 (1958)
80. Reshak, A.H., Auluck, S., Kityk, I.: Electronic band structure and optical properties of $Sr_{n+1}Ti_nO_{3n+1}$ Ruddlesden-Popper homologous series. Jpn. J. Appl. Phys. **47**(7R), 5516 (2008)
81. Lee, C.-H., et al.: Effect of reduced dimensionality on the optical band gap of $SrTiO_3$. Appl. Phys. Lett. **102**(12), 122901 (2013)
82. Li, Y., Zhang, L., Ma, Y., Singh, D.J.: Tuning optical properties of transparent conducting barium stannate by dimensional reduction. APL Mater. **3**(1), 011102 (2015)
83. Sanchez, F., Ocal, C., Fontcuberta, J.: Tailored surfaces of perovskite oxide substrates for conducted growth of thin films. Chem. Soc. Rev. **43**(7), 2272–2285 (2014)
84. Fan, D., et al.: Synergy of photocatalysis and photothermal effect in integrated 0D perovskite oxide/2D MXene heterostructures for simultaneous water purification and solar steam generation. Appl. Catal. B **295**, 120285 (2021)